JOURNAL OF GEOPHYSICAL RESEARCH: SPACE PHYSICS, VOL. 118, 3165–3172, doi:10.1002/jgra.50319, 2013

Quasi-steady, marginally unstable electron cyclotron harmonic wave amplitudes

Xiaojia Zhang,[1] Vassilis Angelopoulos,[1] Binbin Ni,[2] Richard M. Thorne,[2] and Richard B. Horne[3]

Received 21 December 2012; revised 29 April 2013; accepted 4 May 2013; published 18 June 2013.

[1] Electron cyclotron harmonic (ECH) waves have long been considered a potential driver of diffuse aurora in Earth's magnetotail. However, the scarcity of intense ECH emissions in the outer magnetotail suggests that our understanding of the amplification and the relative importance of these waves for electron scattering is lacking. We conduct a comprehensive study of wave growth and quasi-linear diffusion to estimate the amplitude of loss-cone-driven ECH waves once diffusion and growth balance but before convection or losses alter the background hot plasma sheet population. We expect this to be the most common state of the plasma sheet between episodes of fast convection. For any given wave amplitude, we model electron diffusion caused by interaction with ECH waves using a 2-D bounce-averaged Fokker-Planck equation. After fitting the resultant electron distributions as a superposition of multicomponent subtracted bi-Maxwellians, we estimate the maximum path-integrated gain using the HOTRAY ray-tracing code. We argue that the wave amplitude during quasi-steady state is the inflection point on a gain-amplitude curve. During quasi-steady state, ECH wave amplitudes can be significant (~1 mV/m) at $L \sim 8$ but drop to very low values (<~0.1 mV/m) in the outer magnetotail ($L \sim 16$) and likely fall below the sensitivity of typical instrumentation relatively close to Earth mainly because of the smallness of the loss cone. Our result reinforces the potentially important role of ECH waves in driving diffuse aurora and suggests that careful comparison of theoretical wave amplitude estimates and observations is required for resolving the equatorial scattering mechanism of diffuse auroral precipitation.

Citation: Zhang, X.-J., V. Angelopoulos, B. Ni, R. M. Thorne, and R. B. Horne (2013), Quasi-steady, marginally unstable electron cyclotron harmonic wave amplitudes, *J. Geophys. Res. Space Physics*, *118*, 3165–3172, doi:10.1002/jgra.50319.

1. Introduction

[2] Diffuse aurora, a broad band of weak emissions extending around the auroral oval [*Horne et al*., 2003], is a semipermanent feature of the auroral zone. The dominant contributor to hemispheric energy flux precipitating into the ionosphere [*Newell et al*., 2009], diffuse aurora extends over a latitude range of 5° to 10° and maps out to the entire central plasma sheet [*Meredith et al*., 2009]. More than three quarters of the energy flux in diffuse auroral precipitation is contributed by diffuse electron precipitation [*Newell et al*., 2009], which is caused by pitch-angle scattering of plasma sheet electrons in the hundreds to several thousand eV energy range into the atmospheric loss cone by wave-particle interactions [*Fontaine and Blanc*, 1983]. Both electron cyclotron harmonic (ECH) waves and whistler-mode chorus resonate with electrons in this energy range [*Anderson and Maeda*, 1977] and have been considered as mechanisms for plasma sheet electron precipitation.

[3] Electron cyclotron harmonic waves, electrostatic emissions that are usually observed in bands between the harmonics of the electron gyrofrequency [*Kennel et al*., 1970; *Meredith et al*., 2009], have been attributed to the loss-cone instability of the ambient, hot plasma sheet electron distribution [*Ashour-Abdalla and Kennel*, 1978; *Horne et al*., 1981; *Horne*, 1989; *Horne et al*., 2003]. Localized to within a few degrees of the magnetic equator, ECH emissions are seen most frequently in the night and dawn regions (~2100–0600 magnetic local time (MLT)) for $4 < L < 10$ [*Roeder and Koons*, 1989; *Meredith et al*., 2009; *Ni et al*., 2011a].

[4] The relative importance of ECH waves to diffuse auroral precipitation has been controversial for over four decades [e.g., *Kennel et al*., 1970; *Lyons*, 1974; *Belmont et al*., 1983; *Roeder and Koons*, 1989; *Horne and Thorne*,

[1]Department of Earth and Space Sciences, University of California, Los Angeles, California, USA.
[2]Department of Atmospheric and Oceanic Sciences, University of California, Los Angeles, California, USA.
[3]British Antarctic Survey, Natural Environment Research Council, Cambridge, UK.

Corresponding author: X.-J. Zhang, Department of Earth and Space Sciences, University of California, 603 Charles E. Young Dr. E, Los Angeles, CA 90095, USA. (xjzhang@ucla.edu)

2169-9380/13/10.1002/jgra.50319

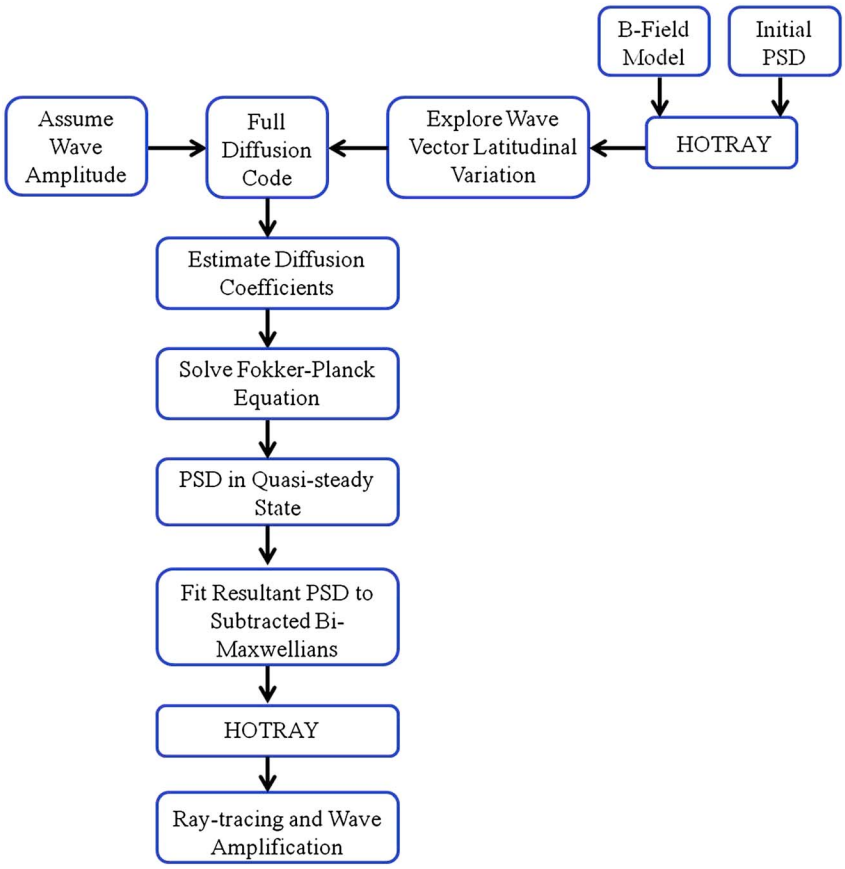

Figure 1. Flow chart of methodology to estimate wave amplification corresponding to the prescribed electric field amplitude. PSD denotes electron phase space density.

2000; *Horne et al*., 2003; *Meredith et al*., 2009]. Recent theoretical and modeling studies [*Thorne et al*., 2010; *Ni et al*., 2011b, 2011c] have shown that whistler-mode chorus waves play a significant role in driving the diffuse aurora in the inner magnetosphere ($<\sim 8\,R_E$). Beyond ~8 R_E, in the night-to-dawn MLT sector where the diffuse auroral activity is also intense, chorus emissions are weak, below about a few pT [*Li et al*., 2009a]. Moderately strong ECH waves (>0.1 mV/m), however, have been reported to extend to ~12 R_E [e.g., *Roeder and Koons*, 1989; *Ni et al*., 2011a]. In a detailed case study, *Ni et al*. [2012a] quantified the rate of central plasma sheet electron scattering by ECH waves at $L = 11.5$ and evaluated the ionospheric precipitation flux and resultant auroral brightness, which agreed with auroral observations at the magnetic foot point. Thus, ECH emissions are potentially significant for understanding the origin of diffuse auroral precipitation in the outer magnetosphere.

[5] The statistical study by *Newell et al*. [2009] revealed contradictory observational evidence regarding the propensity and importance of ECH wave emissions at high L-shells. Diffuse auroral precipitation is both statistically significant and energetically efficient at higher latitudes, since about half the emissions are contributed by precipitation at magnetic latitudes from >65° to ~70° across ~17 hours of magnetic local time (MLT) centered at ~3 MLT [see *Newell et al*., 2009, Figure 5]. These latitudes are expected to map to the outer magnetosphere from $L \sim 8$ to beyond $L \sim 15$. On the other hand, according to *Ni et al*. [2011a], ECH waves at high L-shells (especially >~12, see their Figures 1 and 2) are relatively scarce. Other free energy sources for electron scattering, such as whistler-mode chorus, are also absent at high L-shells [*Li et al*., 2009a]. The observations therefore suggest that although electron scattering into the loss cone persists at high L-shells, the wave mode, excitation mechanism, and amplitude responsible for filling the loss cone and loss-cone properties resulting in the observed precipitation rates are far from understood. Since the electron loss cone still exists in the outer magnetosphere, providing free energy for ECH wave excitation, it is reasonable to assume that these electrostatic waves still exist there. We evaluate ECH wave electric field amplitudes during quasi-steady state at different magnetotail locations using idealized but physically accurate models of the interplay between magnetic field strength and curvature, wave growth and propagation, and electron diffusion and loss-cone evolution, to establish trends that may help explain the above observational discrepancy. We find that ECH wave amplitudes consistent with quasi-steady state decrease with increasing L value and likely fall below the instrument detection level reasonably close to the inner edge of the plasma sheet.

2. Methodology

[6] The methodology to evaluate the wave amplification corresponding to the prescribed electric field amplitude is summarized in the flow chart in Figure 1. It involves repeated

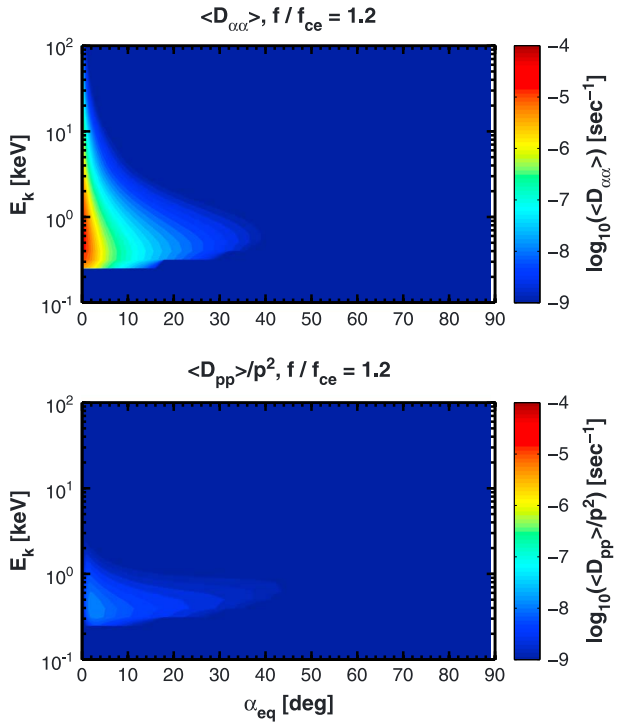

Figure 2. (top) Bounce-averaged pitch-angle and (bottom) momentum diffusion coefficients as a function of equatorial pitch angle and electron kinetic energy due to ECH waves ($L = 16$, $E_w = 0.1$ mV/m).

cycles of the following three steps: modeling the electron diffusion using quasi-linear theory, fitting the electron distribution function, and evaluating the wave amplification using the HOTRAY ray-tracing code.

2.1. Modeling Electron Diffusion Using Quasi-linear Theory

[7] We modeled the evolution of the electron pitch-angle distribution caused by interactions with ECH waves using equation (1), the 2-D bounce-averaged Fokker-Planck equation [*Tao et al*., 2011; *Ni et al*., 2012b], to obtain the electron phase space density (PSD) f in a marginally unstable state

$$\frac{\partial f}{\partial t} = \frac{1}{S_0 \sin\alpha_{eq}\cos\alpha_{eq}} \frac{\partial}{\partial \alpha_{eq}} \left(S_0 \sin\alpha_{eq}\cos\alpha_{eq} \langle D_{\alpha\alpha}\rangle \frac{\partial f}{\partial \alpha_{eq}} \right) + \frac{1}{p^2}\frac{\partial}{\partial p}\left(p^2 \langle D_{pp}\rangle \frac{\partial f}{\partial p}\right) - \frac{f}{\tau} \quad (1)$$

[8] Here p is the particle momentum, α_{eq} is the equatorial pitch angle, S_0 is the bounce period-related term, and $\langle D_{\alpha\alpha}\rangle$ and $\langle D_{pp}\rangle$ are the bounce-averaged pitch-angle and momentum diffusion coefficients, respectively. Mixed diffusion terms $D_{\alpha p}$ were omitted in this equation. The loss time τ is set to one quarter of the bounce period if α_{eq} is less than the local loss-cone angle α_{lc} and infinity otherwise. Our neglect of mixed diffusion terms simplified the algorithm and reduced the computation time, while retaining the dominant diffusion process that affects plasma sheet electrons [e.g., *Albert and Young*, 2005].

[9] To account for the stretched configuration of a realistic magnetotail, we adopted the Dungey magnetic field model [*Dungey*, 1961], which consists of a dipole magnetic field and a uniform southward magnetic field. The stretching of the Dungey field relative to the dipole field is controlled by the intensity of the superimposed southward magnetic field ($B_{z,0}$), described by the parameter $b = (M/B_{z,0})^{1/3}$ (M is the dipole magnetic moment). Smaller b values result in more stretched fields. When b goes to infinity, the Dungey field reduces to a dipole field. The magnetic field-related parameters (S_0 and α_{lc}) in equation (1) were evaluated for this model using the equations given by *Ni et al*. [2012b]. Because the magnetic field intensity in the Dungey field decreases at lower latitudes (within about $\pm 15°$) but increases at higher latitudes compared to the dipole configuration, the loss-cone size (α_{lc}) at a given L-shell is smaller for the Dungey model than for the dipole. In addition, the particle bounce period decreases due to the stretched field lines. The latitudinal wave vector distribution was obtained using the ray-tracing code HOTRAY [*Horne*, 1989] for a fixed wave frequency (we used $f = 1.2 f_{ce}$ for the equatorial wave frequency based on typical values of such waves in the observations). Following *Ni et al*. [2011b, 2012a], we calculated the bounce-averaged diffusion coefficients in the Dungey fields, shown in Figure 2 (for one case at $L = 16$ with wave electric field amplitude $E_w = 0.1$ mV/m), using the UCLA Full Diffusion Code [*Ni et al*., 2008; *Shprits and Ni*, 2009]. Bounce-averaged diffusion coefficients spread over a broader energy and pitch-angle range with a Dungey field than with a dipolar field, and the rates increase, especially at lower energy levels, mainly due to smaller magnetic field intensity. The alternative direction implicit method [*Xiao et al*., 2009; *Tao et al*., 2011] was used to numerically solve equation (1). The initial conditions were taken from Time History of Events and Macroscale Interactions during Substorms (THEMIS) observations, after suppressing anisotropies of the hot component outside the loss-cone, recognizing that such anisotropies are variable and not permanent in the plasma sheet. Boundary conditions for the pitch-angle operator were $\partial f/\partial \alpha_{eq} = 0$ at $\alpha_{eq} = 0°$ and at $\alpha_{eq} = 90°$. For the energy diffusion operator, the lower boundary was held constant at 47 eV because the diffusion timescale of these electrons is much longer than that of typical plasma sheet electrons; the upper boundary was also held fixed at 26 keV, well above typical resonant energies of ECH waves with plasma sheet electrons (hundreds of eV to several keV). Although electron diffusion lasts for hours, basic loss-cone properties are established rather quickly (minutes to tens of minutes); after that, the drainage of electrons at larger pitch angles takes place very slowly, over time scales of many hours to days. We assume that the marginally unstable state has been reached when the electron PSD over potentially resonant energies changes less than 10% in 1 hour.

2.2. Fitting Electron Distribution Function

[10] To evaluate the amplification of ECH emissions using the HOTRAY ray-tracing code, we need to model the PSD of resonant electrons. The electron PSD (f) within the boundaries of potentially resonant energies was fitted as a sum

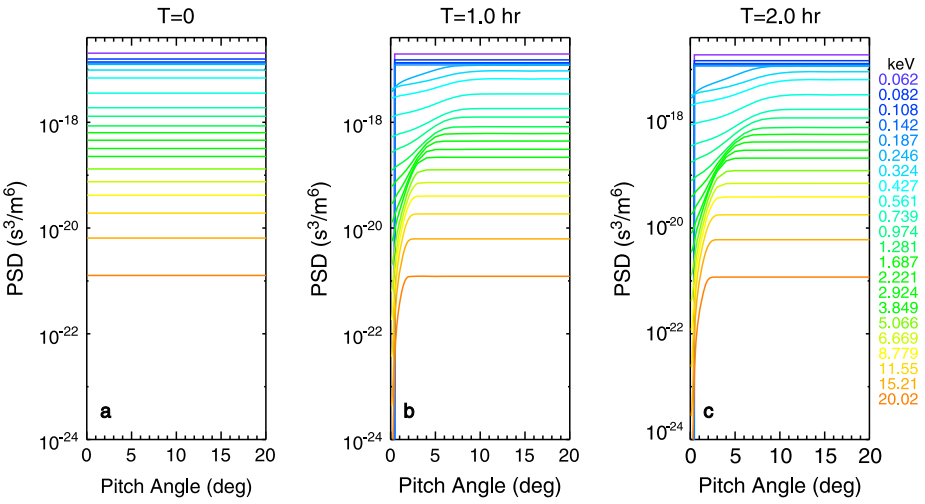

Figure 3. Initial electron distribution (isotropic) for modeling the diffusion process and the evolution of electron distribution after interaction with ECH waves for 1 h and 2 h ($L = 16$, $E_w = 0.1$ mV/m).

of subtracted bi-Maxwellians [e.g., *Ashour-Abdalla and Kennel*, 1978; *Horne et al*., 2003; *Li et al*., 2009b] given by

$$f = \sum_i f_i,$$

where each component is expressed by

$$f_i(v_{//}, v_\perp) = \frac{n_i}{\pi^{2/3}\alpha_{\perp i}^2 \alpha_{//i}} \exp\left(-\frac{v_{//}^2}{\alpha_{//i}^2}\right) \cdot\left[\Delta_i \exp\left(-\frac{v_\perp^2}{\alpha_{\perp i}^2}\right) + \frac{(1-\Delta_i)}{(1-\beta_i)}\cdot\left(\exp\left(-\frac{v_\perp^2}{\alpha_{\perp i}^2}\right) - \exp\left(-\frac{v_\perp^2}{\beta_i \alpha_{\perp i}^2}\right)\right)\right]. \quad (2)$$

[11] Here n_i is the electron density, $\alpha_{\perp i}$ and $\alpha_{//i}$ are the thermal velocities perpendicular and parallel to the ambient magnetic field, and β_i and Δ_i essentially determine the depth and width of the loss cone, respectively.

2.3. Evaluation of Wave Amplification Using HOTRAY Ray-Tracing Code

[12] Using the above-modeled electron distributions and the HOTRAY code, we simulated ECH wave propagation in Dungey fields as follows: At every step along each ray path, the hot plasma dispersion relation for electrostatic ECH waves was solved to obtain amplification of the wave electric field over a ray path **r** (path-integrated gain G in dB) [*Horne and Thorne*, 1997; *Li et al*., 2009b]:

$$G = 20\log_{10}(E/E_0) = 8.6859 \int \mathbf{k}_i \cdot d\mathbf{r} \quad (3)$$

[13] Electron cyclotron harmonic waves typically reflect once they are only a short distance away from the neutral sheet, due to field line bending, which modifies the wave normal angle to the field and thus the group velocity. Because of the larger curvature of the Dungey field configuration, the waves reflect at lower latitudes (closer to the neutral sheet) in a Dungey field than in a dipole field. Furthermore, Dungey field intensity along a ray path is different from that along a ray path in the dipole; this field intensity directly affects the local value of f/f_{ce} and thus the wavenumber and the magnitude of path-integrated gain. For a given electric field amplitude, the electron distribution was first evolved through quasi-linear diffusion to attain a marginally unstable state (Figure 3). Then, using that evolved distribution as an input to the HOTRAY code, nineteen rays were launched from the magnetic equator with the same wave frequency ($1.2 f_{ce}$) and wave normal angle (89.8°), but propagating with different initial azimuthal angles (0°–180° range) and thus into different magnetic field strengths and curvatures. We assume that the gain along the ray path can represent the final amplitude of the wave, in addition to the local wave growth. We also assume that this path-integrated gain dominates over changes in the wave energy density due to divergence of the rays. We thus recorded the maximum path-integrated gain for each azimuthal angle and computed the median value of these nineteen peak gains to represent the maximum amplification corresponding to the prescribed electric field amplitude and its accompanying electron distribution. By varying the wave electric field amplitude over a wide range of reasonable values, we determined the expected amplification (gain) of ECH waves from self-consistently evolved electron distributions.

[14] Only one point on those gain-amplitude curves is expected to be consistent with a given set of ambient plasma sheet conditions for the quasi-steady state. That point is determined as a balance between the local plasma properties (i.e., the dispersion relation) affecting the wave vector, the resonant energies, and resonant particle number densities on the one hand and the properties of the surrounding medium (i.e., field curvature and gradients) controlling propagation, diffusion, and amplification on the other hand. If amplification is lower than what is consistent with the quasi-steady state for these conditions, then the local wave amplitudes will be lower; the electron distribution function will thus develop a deeper/sharper loss cone and then increase the wave growth rates. Consequently, the local amplitude will increase dramatically relative to the quasi-steady state as part of the quasi-linear feedback process. If the local wave amplitude becomes lower than what is consistent with quasi-steady state conditions, then

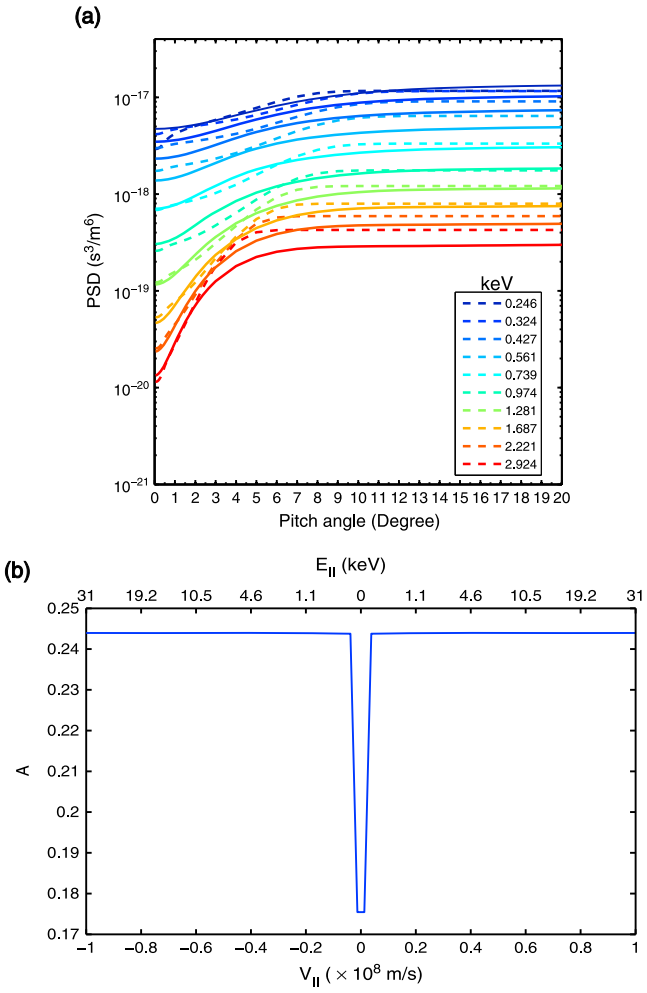

Figure 4. (a) Electron phase space density (PSD) after diffusion as a function of pitch angle for energy levels resonant with ECH waves. The dashed lines display the diffused electron distribution, and solid lines represent electron PSD fitted to multicomponent subtracted bi-Maxwellians. (b) The electron anisotropy as a function of parallel electron velocity/energy.

the loss cone will be depleted and amplification will increase rapidly. For random variations of the medium, the system will settle toward a state of minimum amplitude for a given source and minimum amplification for a given model that are consistent with each other. Thus, the quasi-steady state point for a prescribed set of plasma and medium conditions, which is expected to be an inflection point on the gain-amplitude curve, can be identified from such curves for different L-shells. We define the quasi-steady state as the transition point at which the path-integrated gain curve as a function of wave amplitude changes dramatically from sharply descending to almost flat. Specifically, we linearly fitted the gain-log(amplitude) (G-logA) curve before and after the transition point with two distinct slopes and determined the wave amplitude at the intersection of two fitted lines as the ECH wave amplitude at the quasi-steady state. We examined the G versus A behavior for three different L-shells, $L = 8$, $L = 12$, and $L = 16$.

[15] In each set of runs for a fixed L-shell, the electron distribution was assumed to be constant with latitude and unchanging through the entire propagation region (<~1 R_E). To avoid any variations in the path-integrated gain due to differences in cold electron density, we used the same cold electron density ratio for each set of L-shell runs.

3. Results

[16] In this section, we present our model results of ECH wave amplification at three different L-shells. We used quasi-linear theory to model the evolution of electron pitch-angle distribution due to interactions with ECH waves. Figure 3 shows results for one case at $L = 16$ with wave electric field amplitude $E_w = 0.1$ mV/m ($f/f_{ce} = 1.2$) after interaction with ECH waves for one hour (1h) and two hours (2h). Clearly seen in this figure is that ECH waves can only affect the PSD of electrons with pitch angles <20° over a limited energy range, which is consistent with numerical results by *Thorne et al.* [2010] and *Tao et al.* [2011]. Comparing the evolution of electron distributions at 1 h and 2 h, we see that the shape of the electron distribution was already rather stable except for a slow decrease in the distribution at both low (<0.4°, i.e., inside the loss cone) and relatively high (0.4°–10°) pitch-angle due to precipitation. Thus, we defined this state with stabilized electron pitch-angle distribution as marginally unstable state at this given wave amplitude ($E_w = 0.1$ mV/m). This modeling was applied to all wave amplitudes considered.

[17] The marginally unstable electron PSD from our diffusion calculation was fitted over the resonant energies using equation (2); the result for the specific amplitude and L-shell in Figure 3 is presented in Figure 4. Three components were used to fit the diffused electron pitch-angle distribution in velocity space (PSD in Figure 3c). Because ECH waves affect only electron distributions with pitch angles <20° and these waves are excited by PSD gradients near the loss cone, we only fitted the distributions with pitch angles <20°. Moreover, we increased computational efficiency by fitting only the resonant portion (hundreds eVto3 keV) of the energy spectrum at pitch angles <20° (free energy source). Even without considering the observational constraints on the pitch-angle variation of the distributions, due to the limited angular resolution of current instrumentation, previous modeling studies have been severely affected by the limited capability of a single set of subtracted bi-Maxwellians to fit any realistic loss cone in the outer magnetosphere. Our use of multiple subtracted bi-Maxwellians overcomes those limitations and increases the fidelity of the loss-cone modeling, which provides realistic estimates of the growth rate and the resulting amplification.

[18] The fitting parameters obtained by a constrained nonlinear optimization fit to the diffusion code results are listed in Table 1; these parameters were used as input to the

Table 1. Parameters of Electron Components Used to Model the Diffused Suprathermal Electron Phase Space Density for the Case in Figure 3

Component	$N_e(m^{-3})$	$T_\perp$(eV)	$T_{//}$(eV)	Δ	β
1	3.78×10^4	1.35	1.35	1.0	0.5
2	1.70×10^5	307.4	249.2	0.413	0.014
3	1.70×10^5	1705.2	1382.1	0.047	0.009

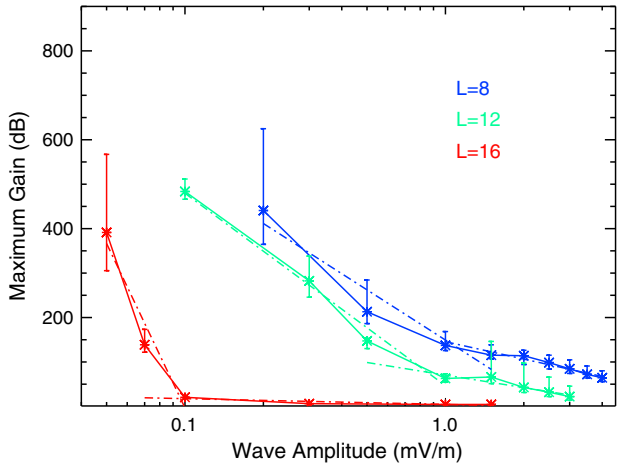

Figure 5. ECH wave amplification corresponding to different wave electric field amplitudes at $L = 8$, $L = 12$, and $L = 16$. Dashed lines were fitted to determine the inflection point corresponding to the quasi-steady state.

HOTRAY code to trace ECH waves and obtain the path-integrated wave gain. As mentioned above, for each assumed wave amplitude at a specified location, we launched nineteen rays from the magnetic equator with the same wave frequency ($1.2 f_{ce}$) and wave normal angle (89.8°), but with various initial azimuthal angles from 0° to 180°. Then the median value of the nineteen maximum gains was recorded to represent the wave amplification corresponding to the prescribed wave amplitude. By varying the diffusion coefficients and magnetic field-related parameters in the first step (section 2.1), we estimated the wave amplification corresponding to each assumed wave electric field amplitude at each L-shell. Figure 5 illustrates the variation of ECH wave amplification with wave electric field amplitude at three L-shells. Error bars show the upper and lower quartiles of the maximum gain at each amplitude value over different azimuthal angles.

[19] To quantitatively evaluate the inflection point in a gain-log(amplitude) curve, we linearly fitted the curve before and after the transition point with two distinct slopes (dashed lines in Figure 5) and defined the wave amplitude at the intersection of two fitted lines as the ECH wave amplitude at the quasi-steady state. From Figure 5, we can see that the ECH wave amplitude consistent with quasi steady state is ~1 mV/m at $L = 8$ but decreases with increasing L-shell. It drops to ~0.8 mV/m at $L = 12$ and descends to ~0.1 mV/m in the outer magnetotail ($L = 16$).

4. Summary and Discussion

[20] We numerically modeled the interaction between electrons and ECH waves to estimate the amplitude of these waves during the quasi-steady state. Quasi-linear theory modeling was used to investigate the evolution of electron pitch-angle distributions due to interaction with ECH waves, from which we obtained the marginally unstable state electron distribution. The quasi-linearly evolved electron distribution (Figure 3) shows that ECH waves only affect the PSD of electrons over a limited energy range with pitch angles <20°, as consistent with previous numerical results [*Thorne et al*., 2010; *Tao et al*., 2011].

[21] After obtaining the diffused electron distribution, we used the HOTRAY ray-tracing code to examine the path-integrated growth of ECH waves. By iteratively varying the wave electric field amplitude and evaluating the corresponding amplification, we determined the quasi-steady state as the transition point in the gain-amplitude curve. In this quasi-steady state, ECH waves diffuse electrons to form a partly filled loss cone distribution that amplifies the waves only moderately. We find that the wave amplitude corresponding to the quasi-steady state decreases with increasing L-shell, from ~1 mV/m at $L = 8$ to ~0.1 mV/m at $L = 16$.

[22] To use the HOTRAY code to evaluate ECH emission amplification, we fitted the diffused electron distribution (Figure 3) with multicomponent subtracted bi-Maxwellians. Discrepancies between the fitted and diffused electron distributions, especially near sharp gradients at the edge of the loss-cone, remain, however, indicating that our modeling cannot be used reliably for very small loss cones ($\alpha_{lc} < 0.4°$ or $B_{eq} < 2$ nT). Furthermore, we used the Dungey magnetic field model, which likely overestimates the electron loss-cone size at high L-shells, to simulate the stretched outer magnetotail. Finally, ray tracing as applied here cannot give a good estimate of local wave amplitudes unless the source is well known and the change of wave energy density due to ray divergence is properly evaluated. Nonetheless, our results establish trends that can be extended outside the limits of our modeling.

[23] Specifically, we found that as we move to higher L-shells, the progressively smaller loss cones at those L-shells can be readily filled through quasi-linear diffusion by smaller wave amplitudes, establishing the quasi-steady state. Although the absolute values of the quasi-steady state amplitude versus L-shell may not be accurate for the reasons explained earlier, our study captures the physics of the problem and establishes a realistic trend. We can reasonably extrapolate that the wave amplitude during the quasi-steady state can eventually drop to below electric field instrument (EFI) sensitivity level (~0.01 mV/m for the THEMIS EFI

Table 2. Assumed Values of Plasma Sheet Electron (100 eV–10 keV) Fluxes From THEMIS Observations and Estimated Precipitated Electron Energy Flux for Relatively Quiet and Active Times With Different Diffusion Extents at $L = 8$, $L = 12$, and $L = 16$, Respectively

	Quiet			Active		
		Estimated Precipitated Energy Flux (ergs/cm^2/s)			Estimated Precipitated Energy Flux (ergs/cm^2/s)	
L	Assumed Energy Flux (eV/cm^2/s/str/eV)	Strong Diffusion	Weak Diffusion	Assumed Energy Flux (eV/cm^2/s/str/eV)	Strong Diffusion	Weak Diffusion
8	1.29×10^6–3.69×10^7	3.6–4.5	0.06–0.07	1.96×10^6–4.60×10^7	3.7–6.9	0.06–0.11
12	1.68×10^6–4.66×10^7	1.8–7.0	0.20–0.77	1.88×10^6–6.01×10^7	9.6–18.4	1.06–2.02
16	4.11×10^5–1.99×10^7	3.9–5.9	0.94–1.42	1.68×10^5–4.50×10^7	5.7–11.8	1.37–2.83

instrument) under a realistic field. In fact, our model's limitations (Dungey field insufficiently stretched, actual equatorial field smaller than modeled for a stretched magnetotail) suggest that quasi-steady state amplitudes may fall below sensitivity level as close as $L \sim 10$. At $L \sim 10$, the equatorial field is often ~1–5 nT, ~10 times smaller than a dipole's, and the field line radius of curvature is $<1\,R_E$, ~3 times smaller than a dipole's. The ubiquity of the free energy source (incompletely filled loss-cone distribution) further supports our hypothesis that ECH waves can persist in the outer magnetosphere, but with amplitudes possibly below instrument noise level.

[24] While recent theoretical and modeling studies [*Thorne et al*., 2010; *Ni et al*., 2011b, 2011c] have implied that whistler-mode chorus waves play a dominant role in driving diffuse aurora in the inner magnetosphere ($<\sim 8\,R_E$), ECH emissions have been identified as the potential driver of diffuse auroral precipitation in the outer magnetosphere [*Ni et al*., 2011a, 2012a]. The seeming contradiction between the presence of diffuse auroral precipitation at higher latitudes (up to about 70° magnetic latitude) [*Newell et al*., 2009] and the relative scarcity of ECH waves in high L-shells ($>\sim 12$) was addressed in our paper. Our results suggest that such ECH emissions at high L-shells ($L > \sim 12$) are present often, if not always, and can thus be responsible for the observed precipitation, even though evidence of these waves may be scarce at current data sets due to their small amplitudes. For a more quantitative analysis, we can use realistic values of plasma sheet electron fluxes at the peak flux energy (100 eV–10 keV) from THEMIS observations (see, e.g., THEMIS overview plots) and the average loss-cone fill ratio computed from the modeled diffusion process. We thus estimated the precipitated electron energy flux resulting from ECH waves during the quasi-steady state (weak diffusion limit) at $L = 8$, $L = 12$, and $L = 16$, respectively, for relatively quiet times and active times. Our results are shown in Table 2. The strong diffusion case made by assuming distributions isotropic within ~30° in pitch angle away from field aligned, including across the loss cone, was also included in Table 2. The variability of this estimated precipitating energy flux is noticeably large (a factor of ~3.0) because of transient activations (injections associated with bursty bulk flows) that apparently continue even during relatively quiet times [e.g., *Angelopoulos et al*., 1994]. The trends with L-shell are not necessarily representative, as we have used only a small dataset to determine typical energy flux for this analysis. However, it is instructive that the estimated precipitating energy flux agrees with *Newell et al*.'s [2009] statistical estimates of this flux at ionospheric altitudes, including at high L-shells. This suggests that our estimates of the quasi-steady state amplitudes are reasonable. Note that in Table 2, we assumed the same weak diffusion fill ratios for both quiet and active times, namely, those determined from our quasi-steady state solution. The loss-cone filling and associated precipitation as a function of L and MLT, subject to observational constraints and under a variety of activity levels, will be investigated in a similar self-consistent manner in future studies.

[25] **Acknowledgments.** We thank L. Chen and X. Tao for useful discussions. We also thank J. Hohl for her help with editing. We acknowledge NASA contracts NAS5-02099 and NNX12AD12G.

[26] Masaki Fujimoto thanks Yue Chen and another reviewer for their assistance in evaluating this paper.

References

Albert, J. M., and S. L. Young (2005), Multidimensional quasi-linear diffusion of radiation belt electrons, *Geophys. Res. Lett.*, *32*, L14110, doi:10.1029/2005GL023191.

Anderson, R. R., and K. Maeda (1977), VLF emissions associated with enhanced magnetospheric electrons, *J. Geophys. Res.*, *82*(1), 135–146.

Angelopoulos, V., C. F. Kennel, F. V. Coroniti, R. Pellat, M. G. Kivelson, R. J. Walker, C. T. Russell, W. Baumjohann, W. C. Feldman, and J. T. Gosling (1994), Statistical characteristics of bursty bulk flow events, *J. Geophys. Res.*, *99*(A11), 21,257–21,280, doi:10.1029/94JA01263.

Ashour-Abdalla, M., and C. F. Kennel (1978), Nonconvective and convective electron cyclotron harmonic instabilities, *J. Geophys. Res.*, *83*(A4), 1531–1543.

Belmont, G., D. Fontaine, and P. Canu (1983), Are equatorial electron cyclotron waves responsible for diffuse auroral electron precipitation?, *J. Geophys. Res.*, *88*(A11), 9163–9170, doi:10.1029/JA088iA11p09163.

Dungey, J. W. (1961), Interplanetary magnetic field and the auroral zones, *Phys. Rev. Letts.*, *6*, 47–48.

Fontaine, D., and M. Blanc (1983), A theoretical approach to the morphology and the dynamics of diffuse auroral zones, *J. Geophys. Res.*, *88*(A9), 7171–7184.

Horne, R. B. (1989), Path-integrated growth of electrostatic waves: The generation of terrestrial myriametric radiation, *J. Geophys. Res.*, *94*(A7), 8895–8909, doi:10.1029/JA094iA07p08895.

Horne, R. B., and R. M. Thorne (1997), Wave heating of He^+ by electromagnetic ion cyclotron waves in the magnetosphere: Heating near the H^+-He^+ bi-ion resonance frequency, *J. Geophys. Res.*, *102*(A6), 11457–11471, doi:10.1029/97JA00749.

Horne, R. B., and R. M. Thorne (2000), Electron pitch angle diffusion by electrostatic electron cyclotron harmonic waves: The origin of pancake distributions, *J. Geophys. Res.*, *105*(A3), 5391–5402.

Horne, R. B., P. J. Christiansen, M. P. Gough, K. G. Rönnmark, J. F. E. Johnson, J. Sojka, and G. L. Wrenn (1981), Amplitude variations of electron cyclotron harmonic waves, *Nature*, *294*, 338–340, doi:10.1038/294338a0.

Horne, R. B., R. M. Thorne, N. P. Meredith, and R. R. Anderson (2003), Diffuse auroral electron scattering by electron cyclotron harmonic and whistler mode waves during an isolated substorm, *J. Geophys. Res.*, *108*(A7), 1290, doi:10.1029/2002JA009736.

Kennel, C., F. Scarf, R. Fredricks, J. McGehee, and F. Coroniti (1970), VLF electric field observations in the magnetosphere, *J. Geophys. Res.*, *75*(31), 6136–6152.

Li, W., R. M. Thorne, V. Angelopoulos, J. Bortnik, C. M. Cully, B. Ni, O. LeContel, A. Roux, U. Auster, and W. Magnes (2009a), Global distribution of whistler-mode chorus waves observed on the THEMIS spacecraft, *Geophys. Res. Lett.*, *36*, L09104, doi:10.1029/2009GL037595.

Li, W., R. M. Thorne, V. Angelopoulos, J. W. Bonnell, J. P. McFadden, C. W. Carlson, O. LeContel, A. Roux, K. H. Glassmeier, and H. U. Auster (2009b), Evaluation of whistler-mode chorus intensification on the nightside during an injection event observed on the THEMIS spacecraft, *J. Geophys. Res.*, *114*, A00C14, doi:10.1029/2008JA013554.

Lyons, L. (1974), Electron diffusion driven by magnetospheric electrostatic waves, *J. Geophys. Res.*, *79*(4), 575–580.

Meredith, N. P., R. B. Horne, R. M. Thorne, and R. R. Anderson (2009), Survey of upper band chorus and ECH waves: Implications for the diffuse aurora, *J. Geophys. Res.*, *114*, A07218, doi:10.1029/2009JA014230.

Newell, P. T., T. Sotirelis, and S. Wing (2009), Diffuse, monoenergetic, and broadband aurora: The global precipitation budget, *J. Geophys. Res.*, *114*, A09207, doi:10.1029/2009JA014326.

Ni, B., R. M. Thorne, Y. Y. Shprits, and J. Bortnik (2008), Resonant scattering of plasma sheet electrons by whistler-mode chorus: Contribution to diffuse auroral precipitation, *Geophys. Res. Lett.*, *35*, L11106, doi:10.1029/2008GL034032.

Ni, B., R. Thorne, J. Liang, V. Angelopoulos, C. Cully, W. Li, X. Zhang, M. Hartinger, O. Le Contel, and A. Roux (2011a), Global distribution of electrostatic electron cyclotron harmonic waves observed on THEMIS, *Geophys. Res. Lett.*, *38*, L17105, doi:10.1029/2011GL048793.

Ni, B., R. M. Thorne, R. B. Horne, N. P. Meredith, Y. Y. Shprits, L. Chen, and W. Li (2011b), Resonant scattering of plasma sheet electrons leading to diffuse auroral precipitation: 1. Evaluation for electrostatic electron cyclotron harmonic waves, *J. Geophys. Res.*, *116*, A04218, doi:10.1029/2010JA016232.

Ni, B., R. M. Thorne, N. P. Meredith, R. B. Horne, and Y. Y. Shprits (2011c), Resonant scattering of plasma sheet electrons leading to diffuse auroral precipitation: 2. Evaluation for whistler mode chorus waves, *J. Geophys. Res.*, *116*, A04219, doi:10.1029/2010JA016233.

Ni, B., J. Liang, R. M. Thorne, V. Angelopoulos, R. B. Horne, M. Kubyshkina, E. Spanswick, E. F. Donovan, and D. Lummerzheim (2012a), Efficient diffuse auroral electron scattering by electrostatic electron cyclotron harmonic waves in the outer magnetosphere: A detailed case study, *J. Geophys. Res.*, *117*, A01218, doi:10.1029/2011JA017095.

Ni, B., R. M. Thorne, and Q. Ma (2012b), Bounce-averaged Fokker-Planck diffusion equation in non-dipolar magnetic fields with applications to the Dungey magnetosphere, *Ann. Geophys.*, *30*, 733–750, doi:10.5194/angeo-30-733-2012.

Roeder, J. L., and H. C. Koons (1989), A survey of electron cyclotron waves in the magnetosphere and the diffuse auroral electron precipitation, *J. Geophys. Res.*, *94*(A3), 2529–2541.

Shprits, Y. Y., and B. Ni (2009), Dependence of the quasi-linear scattering rates on the wave normal distribution of chorus waves, *J. Geophys. Res.*, *114*, A11205, doi:10.1029/2009JA014223.

Tao, X., R. M. Thorne, W. Li, B. Ni, N. P. Meredith, and R. B. Horne (2011), Evolution of electron pitch angle distributions following injection from the plasma sheet, *J. Geophys. Res.*, *116*, A04229, doi:10.1029/2010JA016245.

Thorne, R. M., B. Ni, X. Tao, R. B. Horne, and N. P. Meredith (2010), Scattering by chorus waves as the dominant cause of diffuse auroral precipitation, *Nature*, *467*, 943–946, doi:10.1038/nature09467.

Xiao, F., Z. Su, H. Zheng, and S. Wang (2009), Modeling of outer radiation belt electrons by multidimensional diffusion process, *J. Geophys. Res.*, *114*, A03201, doi:10.1029/2008JA013580.